Supplementary information (SI)

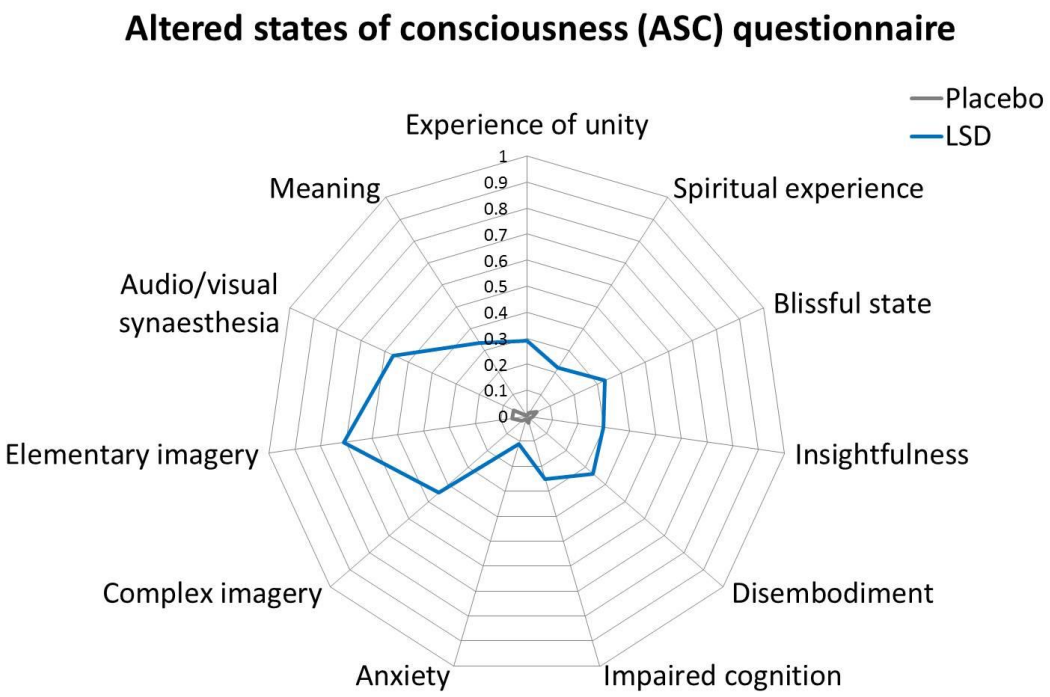

Fig. S1. The 11 factor ASC was completed at the end of scanning days and is presented here as a radar plot with mean total values (0-1) for the LSD (blue) and placebo conditions (gray). Ten of the 11 factors were rated significantly higher under LSD than placebo ($p < 0.05/11$, Bonferonni corrected), with "anxiety" as the exception. See Figures S2 and S3 for additional subjective ratings.

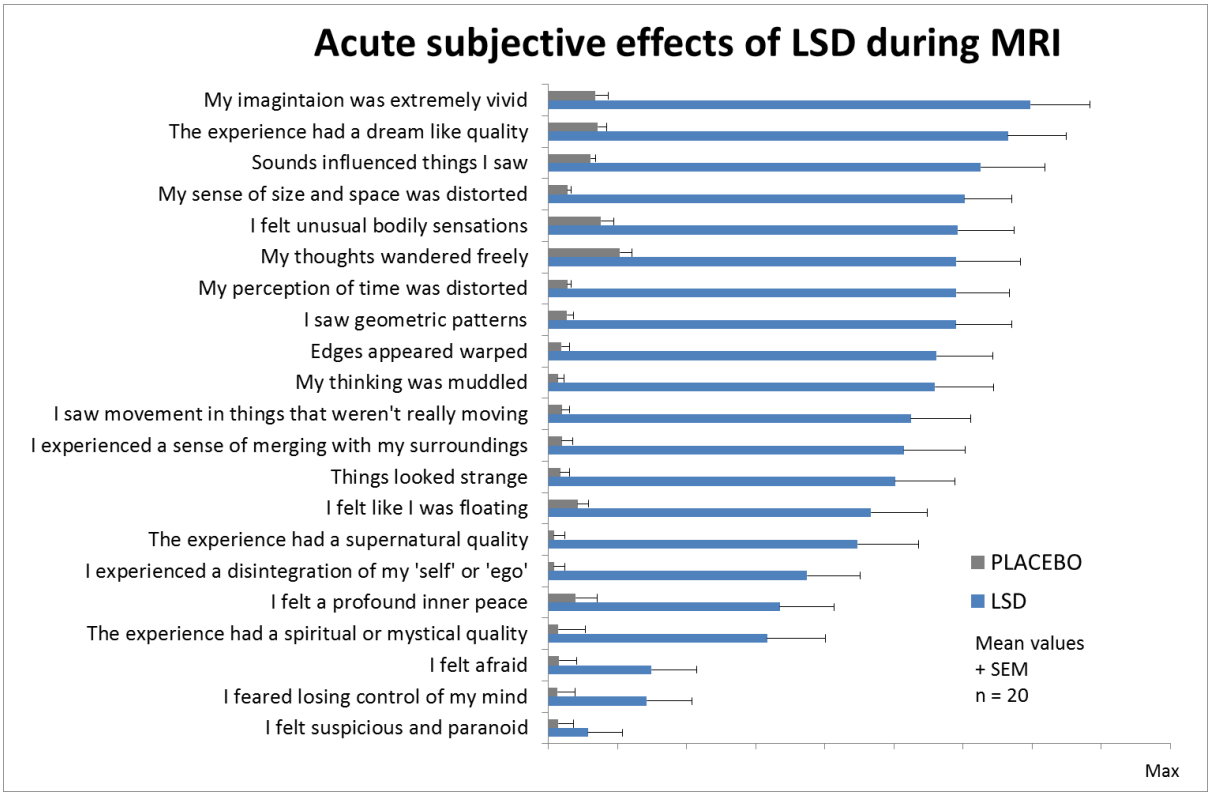

Fig. S2. Additional VAS-style ratings completed directly after MRI scanning ranked by intensity. All items were rated significantly higher under LSD with the exception of the bottom three ($p < 0.05/21$, Bonferonni corrected). A control item "I felt entirely normal" (not shown) was rated higher under placebo than LSD. Items are scored and displayed in a consistent way to the ASC (i.e. 0-1 or % max score).

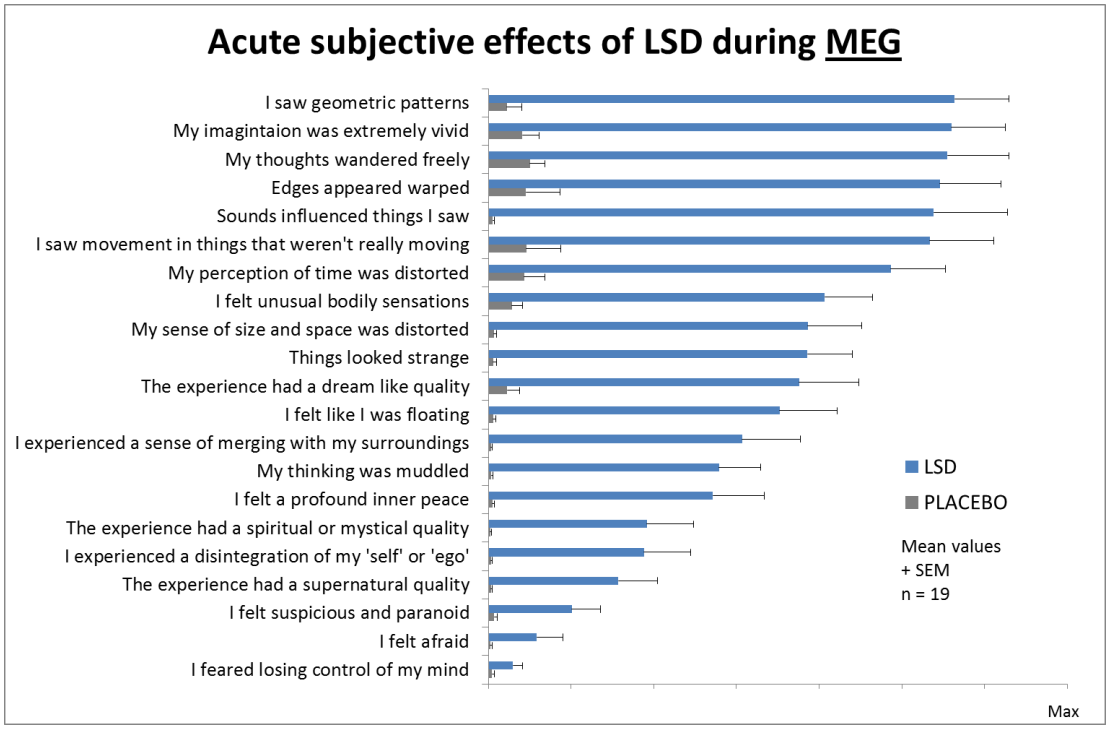

Fig. S3. Additional VAS-style ratings completed directly after MEG scanning ranked by intensity. All items, except the bottom six, were rated significantly higher under LSD than placebo ($p < 0.05/21$, Bonferonni corrected). A control item "I felt entirely normal" (not shown) was rated higher under placebo than LSD. Items are scored and displayed in a consistent way to the ASC (i.e. 0-1 or % max score).

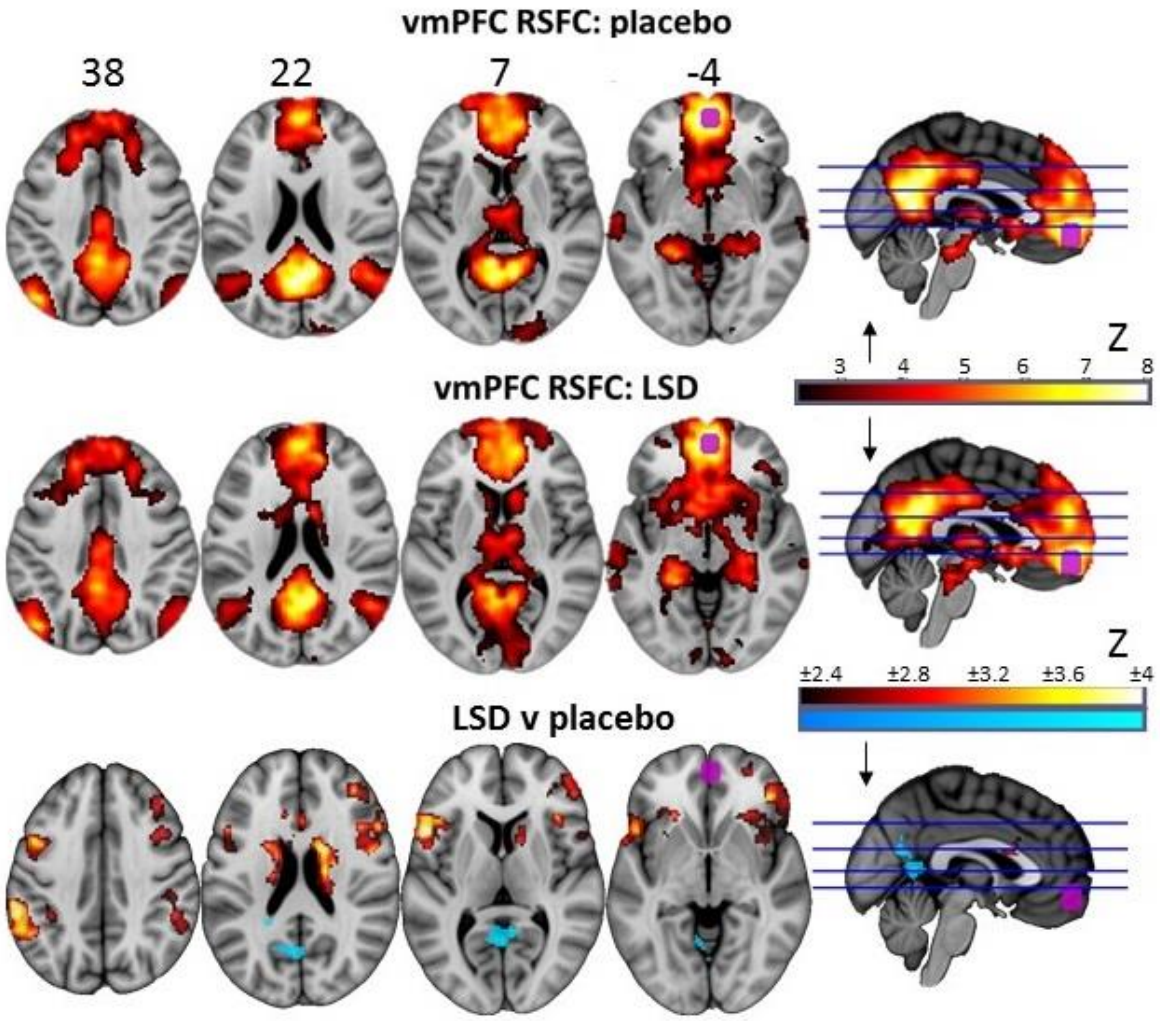

Fig. S4. vmPFC RSFC, z-stat maps ($p < 0.05$, cluster-corrected), seed in purple. The blue horizontal lines on the sagittal sections give the locations of the preceding axial slices. Bottom row = significant between-condition differences in RSFC between the vmPFC seed and the rest of the brain. Blue = decreases and orange = increases in vmPFC RSFC under LSD. All analyses used cluster correction, $p < 0.05$. Note: the left side of the brain is displayed on the left in all of the presented brain images. Unthresholded maps can be viewed in the following link http://neurovault.org/collections/FBVSAVDQ/, n = 15.

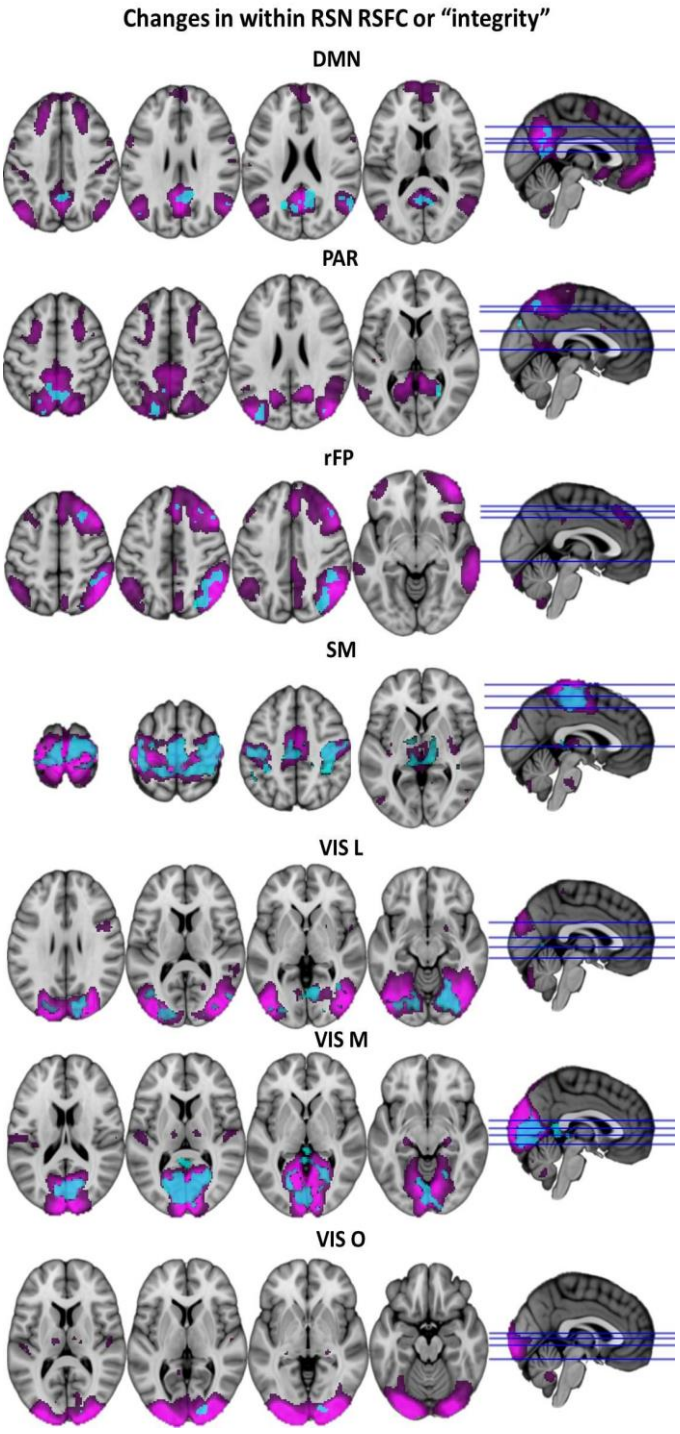

Fig. S5. Decreased RSN integrity under LSD for the 7 RSNs that showed this effect to a significant degree. Purple = RSN, light blue = decreased RSFC ($p < 0.05$, 5000 permutations). For the mean % decrease in integrity within each RSN, see Fig. 2 of the main paper (blue bar), n = 15.

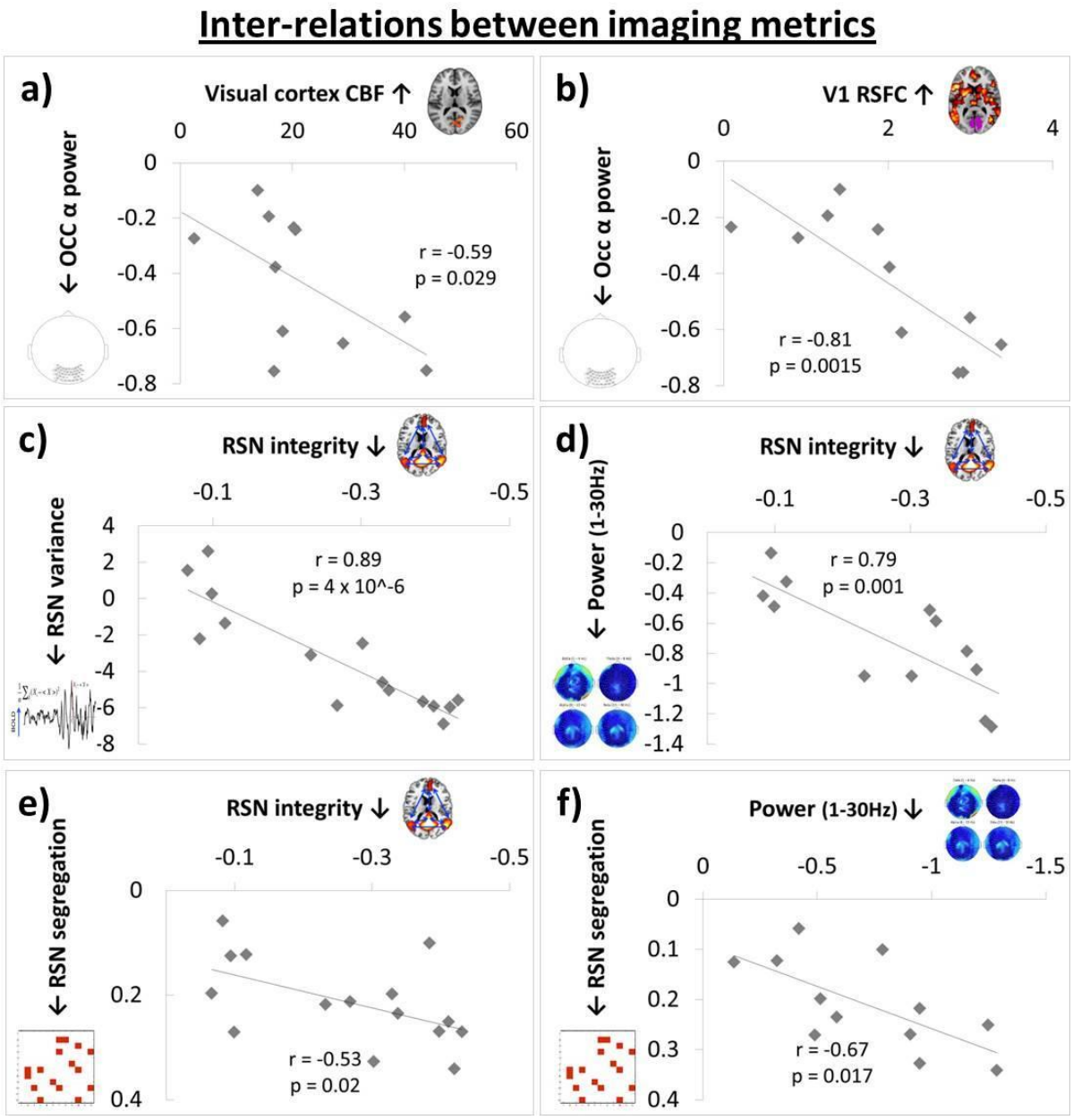

Fig. S6. Relationships between imaging outcomes: **A)** Increased CBF in the visual cortex correlated with decreased alpha power (log (LSD/Placebo)) in occipital cortex sensors. **B)** Increased V1 RSFC correlated with decreased alpha power in occipital cortex sensors. **C)** Decreased RSN integrity (mean of 12 RSNs) correlated with decreased signal variance within these same RSNs (mean of 12 RSNs). **D)** Decreased RSN integrity (mean of 12 RSNs)

correlated with the mean decreases in oscillatory power in the 4 frequency bands ranging from delta (1-4Hz) to beta (13-30Hz). **E)** Decreased RSN integrity (mean of 12 RSNs) correlated with decreased RSN segregation (synonymous with increased between-RSN RSFC and increased RSN desegregation). Mean values for the 8 RSN pairs that showed this effect were used in this correlation. **F)** Decreased RSN segregation (mean of 8 RSN pairs) correlated with decreased power (mean of 4 bands, delta-beta, 1-30Hz). The small graphics on the axes are intended to assist comprehension of the relevant metrics and the arrows indicate the direction of the effect (i.e. a downward arrow indicates a decrease under LSD); n = 11 for a,b (MEG and fMRI), n = 15 for c,d,e,f (fMRI only).

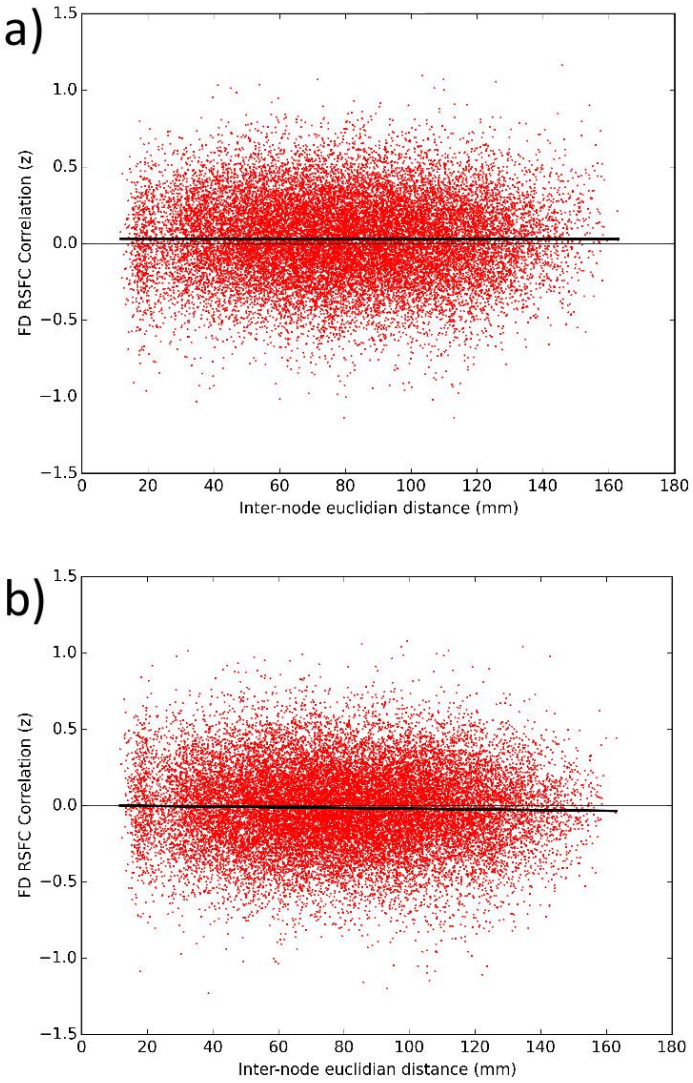

Fig. S7. Correlation between inter-node Euclidian distance (mm) and FD-RSFC correlation (r) for both LSD (a) and placebo (b) after pre-processing. Nodes were defined using the Craddock atlas with 240 parcellations, excluding supplementary motor and motor areas. For each pair of nodes, RSFC was calculated with pearson's r and transformed into z using fisher's transformation. For each pair of nodes, a correlation across subjects was calculated between mean FD and RSFC (r) and transformed into z using fisher's transformation. This correlation is plotted against the distance between nodes (mm). The correlations for LSD and placebo were r = -0.0009 ($p = 0.089$) and r = -0.025 ($p < 0.001$), respectively, suggesting that motion did not affect RSFC in a distant dependant manner after pre-processing.

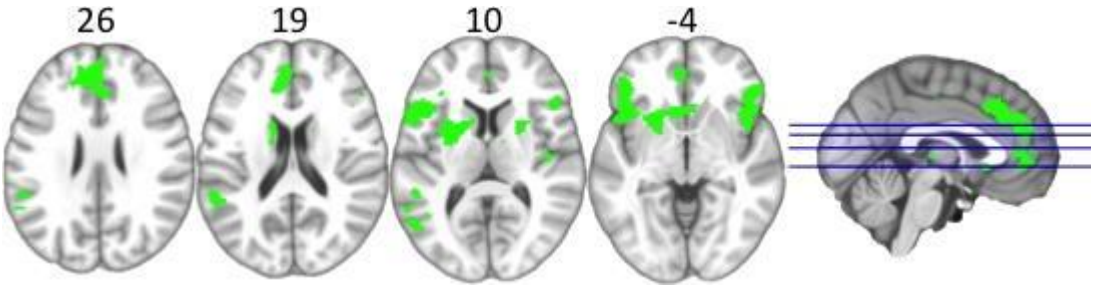

Fig. S8. Increases of V1 RSFC to most significant regions. In order to correlate the increases of V1 RSFC with subjective ratings, we needed to retrieve one z value for all of the (significantly increased) regions. The significant areas with $p < 0.05$ are too widespread for this purpose, we therefore used a threshold of $p < 0.01$ (5000 permutations) to define the most significant regions and subsequently derived the mean z value across all of these regions. A binarized mask of these regions is presented in this figure.

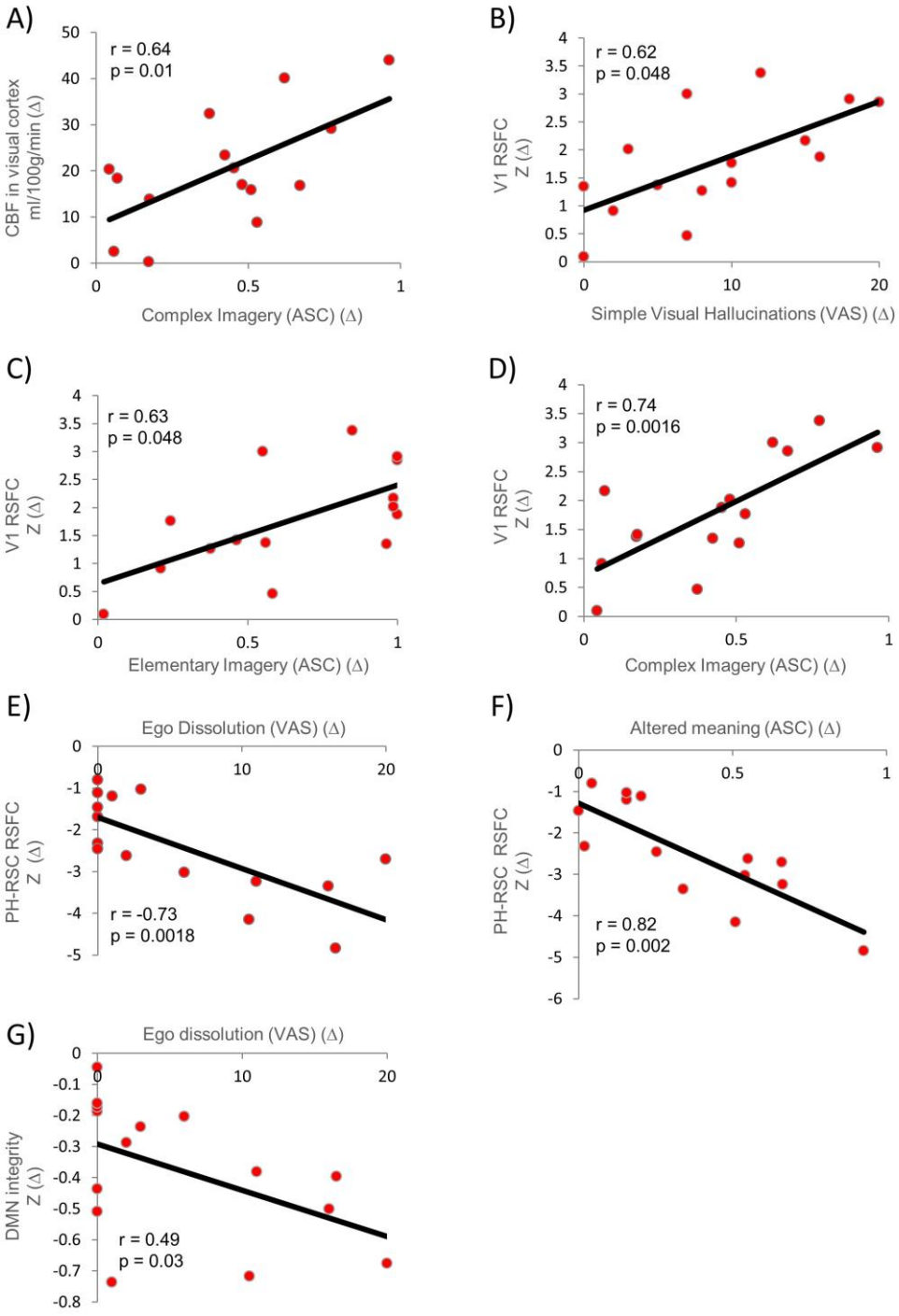

Fig. S9. Correlations between fMRI results and subjective ratings; p values of A and B are bonferroni corrected by 4 (4 visual 'hallucination' items) and p value of C is corrected by 11 (11 ASC dimensions).

VAS Ratings		End of ASL scans (100 mins post inj.)	End of BOLD scans (135 mins post inj.)	End of EC MEG scans (225 mins post inj.)
LSD (mean + SEM)	Intensity	11.7 (0.8)	12.4 (0.9)	6.6 (0.8)
	Simple hallucinations	10.4 (1.7)	9.9 (1.5)	6.5 (1.3)
	Complex hallucinations	8.0 (1.6)	7.4 (1.7)	4.3 (1.1)
	Emoitional arousal	10.6 (0.9)	11.2 (1.2)	6.4 (1)
	Positive mood	7.8 (1.4)	7.0 (1.5)	5.3 (1)
	Ego-dissolution	4.4 (1.3)	5.7 (1.7)	3.3 (1.1)
Placebo (mean + SEM)	Intensity	0.2 (1.8)	0.2 (0.15)	0.17 (0.14)
	Simple hallucinations	0.17 (0.1)	0.17 (1.0)	0.1 (0.04)
	Complex hallucinations	0.1 (0.9)	0.03 (0.03)	0 (0)
	Emoitional arousal	0.9 (0.3)	0.8 (0.3)	0.8 (0.35)
	Positive mood	0.7 (0.3)	0.3 (0.15)	0.4 (0.25)
	Ego-dissolution	0.2 (0.2)	0 (0)	0 (0)

Table S1. Table displays mean values (possible range = 0-20, increments = 1) and positive standard errors for VAS ratings completed at 3 different time points post LSD and placebo injection. See "subjective ratings" below for more details regarding the items. Ratings were visually presented after each scan (on a projection screen visible from within the scanner) and completed via button press. All items, in all 3 modalities, were rated significantly higher under LSD than placebo ($p < 0.05/6$, Bonferonni corrected, methods). EC = eyes closed.

	VisM	VisL	VisO	AUD	SM	DMN	RSP	DAN	SAL	pOP	rFP	lFP
Pearson's r	-0.390	-0.145	-0.025	-0.127	-0.002	-0.490	0.139	0.049	0.386	-0.255	-0.143	-0.300
p (1-tail)	0.076	0.303	0.465	0.325	0.497	0.032	0.689	0.569	0.922	0.179	0.305	0.139

Table S2. Independent correlations between decreased integrity of 12 RSNs and the VAS item "I experienced a dissolution of my 'self' or 'ego'". Only decreased integrity within the DMN correlated significantly with ego-dissolution (see main paper).

V1 RSFC					MNI_152 Cordinates		
	Volume(mm^3)	Difference; Max (z)	Placebo (z)	LSD (z)	x	y	z
Paracingulate/ACC	14912	4.95	1.13	5.85	47	85	48
Left Insula/IFG/Operculum	6992	4.72	1.55	4.75	62	77	26
Left Striatum/Subcallosal	5824	4.36	1.78	5.86	47	72	34
Left Supramarginal/Angular	5616	4.22	1.26	5.6	71	40	44
Right Insula/IFG/Operculum	5136	4.11	-0.93	3.72	23	69	35
MCC	2496	4.16	0.96	4.19	44	58	58
Right Supramarginal/Angular	2128	3.84	0.5	4.6	12	41	46
Right Lateral Occipital	2064	4.17	2.74	4.35	23	29	39
Right Striatum	2040	3.88	1.27	4.5	39	61	44
Posterior Thalamus	1296	4.76	3.22	6.42	47	52	38
Left Precuneus	1264	3.75	0.01	4.19	51	34	56
Left Frontal Pole	984	3.72	-0.26	3.92	58	92	48
Right Heschl's Gyrus	896	3.92	2.06	4.99	23	55	41
Cuneal	480	4.25	2.75	4.63	52	24	53
Left Precentral/NFG	400	3.46	1.55	5.04	71	67	55
Right Precuneus	360	3.82	-1.21	4.18	37	34	53
Left Planum Polare	344	3.48	0.19	3.6	66	52	35
Left Heschl's Gyrus	304	3.4	1.97	5.29	67	52	43
Right MFG	240	3.38	0.255	4.06	20	68	56
Right Putaman	224	3.98	0.21	4.11	33	63	34
Paracingulate	160	3.2	0.95	4.12	49	70	60
Right Putaman	160	3.28	1.93	5.05	35	70	34

Table S3. Regions showing increased V1 RSFC ($p < 0.05$, cluster corrected). All changes were in the direction of increased V1 RSFC under LSD. Note: for tables 2-4, in order to get more segregated clusters, the cluster threshold was set to Z>3 (unlike the figures in the paper, in which Z>2.3). Furthermore, only clusters that were bigger than an arbitrary 20 voxels are reported. The placebo and LSD columns report the z value of each condition separately in the same point as Max.

PH RSFC					MNI_152 Cordinates		
	Volume(mm^3)	Difference; Max (z)	Placebo (z)	LSD (z)	x	y	z
SFG/Paracingulate	1024	3.87	-1.47	2.23	44	84	55
Right MFG	968	3.73	-2.56	1.63	23	71	57
PCC/Precuneus/RSP/Lingual	11760	-5.01	6.43	3.8	36	39	40
Right Hippocampus	296	-3.81	7.14	4.69	29	51	31

Table S4. Regions showing increased (positive z values) and decreased (negative z values) PH RSFC under LSD.

vmPFC RSFC	Volume(mm^3)	Difference; Max (z)	Placebo (z)	LSD (z)	MNI_152 Cordinates		
					x	y	z
Left Supramarginal/Angular	2968	4.58	-3.13	0.42	75	39	51
Left Insula/IFG	2792	4.53	-3.08	0.34	71	71	40
Right Caudate	1448	4.55	-1.27	3.6	37	65	46
Right Insula/IFG	1408	4.18	-5.31	-2.99	18	70	43
Right Supramarginal/Angular	1080	4.02	-4.76	-2.71	14	46	61
Right MFG	944	3.55	-3.2	0.35	28	78	52
Right Frontal Pole	928	4.13	-3.46	1.75	23	82	35
Left Caudate	712	3.71	-2.7	3.19	53	62	48
Right Ftrontal Orbital	592	3.64	0.65	4.36	32	76	32
Left MFG	464	3.89	-4.03	-1.52	68	66	56
Right Precentral	416	4.02	-5.24	-2.43	64	61	58
PCC/Precuneus	192	-4.21	7.15	6.18	45	35	40
PCC/Precuneus	176	-3.43	8.07	6.88	47	31	46

Table S5. Regions showing increased (positive z values) and decreased (negative z values) vmPFC RSFC under LSD.

		pearson r	p (1-tail)			pearson r	p (1-tail)
RSN Integrity	VisM	0.1954	0.7573	RSN Variance	VisM	0.2358	0.8013
	VisL	0.0868	0.6208		VisL	0.3659	0.9101
	VisO	0.5683	0.9865		VisO	0.2440	0.8096
	AUD	0.3806	0.9192		AUD	0.4070	0.9339
	SM	0.3265	0.8825		SM	0.3430	0.8946
	DMN	-0.2809	0.1552		DMN	0.3396	0.8922
	PAR	0.0310	0.5437		PAR	0.4240	0.9424
	DAN	-0.3110	0.1296		DAN	0.1687	0.7261
	SAL	0.2896	0.8525		SAL	0.3745	0.9154
	pOP	-0.2052	0.2316		pOP	0.3427	0.8944
	rFP	-0.0727	0.3984		rFP	0.3337	0.8879
	lFP	-0.2192	0.2163		lFP	0.4399	0.9496
vmPFC RSFC	PCC	**-0.4793**	***0.0353**	RSN Segregation	VisL-PAR	0.0771	0.3924
	Angular	-0.2513	0.8169		VisL-DAN	-0.0436	0.5614
	Striatum	-0.3780	0.9176		VisO-pOP	-0.1539	0.7081
	IFG	-0.0510	0.5717		AUD-PAR	0.3202	0.1223
	All Increases	-0.2323	0.7976		AUD-rFP	-0.0181	0.5255
V1 RSFC	Angular	**0.5573**	***0.0154**		DMN-SAL	-0.2265	0.7915
	Striatum	-0.2075	0.7710		PAR-pOP	0.4248	0.0573
	Paracingulate	0.0845	0.3822		pOP-rFP	-0.1084	0.6497
	IFG&Insula	0.2536	0.1808		VisO-rFP	0.3901	0.0753
	All Increases	0.2554	0.1792				
PH RSFC	PCC&RSP	-0.1834	0.2565				
	SFG	0.1300	0.3221				
	rMFG	0.0163	0.4770				
	All Increases	0.0873	0.3785				

Table S6. Correlations between imaging outcomes and motion (framewise displacement, FD). Very few outcomes correlated significantly with motion but those that did are emboldened and marked with an asterisk.

ASC ratings			Experience of Unity	Spiritual Experience	Blissful State	Insight-fulness	Disem-bodiment	Impaired Cognition	Anxiety	Complex Imagery	Elementary Imagery	Audio/Visual Synaesthesia	Meaning
Difference between correlations with V1-RSFC	Pearson r with Increased V1 RSFC		0.399	0.261	0.371	0.474	0.233	0.188	0.406	**0.739**	**0.629**	**0.644**	0.367
	Differce between V1 RSFC-Complex Imagery correlation and correlations with other ASC items	Z	1.791	2.063	1.734	1.400	2.300	2.487	1.615		0.595	0.636	2.075
		p	***0.036**	***0.019**	***0.041**	0.081	***0.010**	***0.006**	0.053		0.276	0.262	***0.019**
	Differce between V1 RSFC-Elementry Imagery correlation and correlations with other ASC items	Z	0.750	0.992	0.840	0.553	1.505	1.624	0.938	-0.595		-0.075	0.851
		p	0.227	0.161	0.200	0.290	0.066	0.052	0.174	0.276		0.470	0.197
Difference between correlations with PH-RSFC	Pearson r with decreased PH-PCC&RSC RSFC		-0.483	-0.431	-0.405	-0.427	-0.317	-0.113	-0.070	-0.526	-0.052	-0.559	**-0.816**
	Differce between PH RSFC-Altered Meaning correlation and correlations with other ASC items	Z	-2.368	-2.520	-2.617	-2.508	-2.666	-3.000	-2.920	-1.881	-2.739	-1.444	
		p	***0.008**	***0.006**	***0.004**	***0.006**	***0.004**	***0.001**	***0.002**	***0.030**	***0.003**	0.074	
Difference between correlations with CBF in visual area	Pearson r with increased CBF in visual area		0.101	-0.111	0.036	0.148	0.340	0.363	0.303	**0.637**	0.376	0.460	0.272
	Differce between CBF-Complex Imagery correlation and correlations with other ASC items	Z	2.456	2.847	2.453	2.196	1.227	1.170	1.432		1.114	0.984	1.816
		p	***0.007**	***0.002**	***0.007**	***0.014**	0.110	0.121	0.076		0.133	0.163	***0.035**

VAS ratings			Complex Hallucinations	Simple Hallucinations	Emotional Arousal	Positive Mood	Ego Dissolution
Difference between correlations V1-RSFC	Pearson r with Increased V1 RSFC		0.425	**0.627**	0.088	0.200	0.272
	Differce between V1 RSFC-Simple Hallucinations correlation and correlations with other VAS items	Z	2.053		1.677	2.352	1.362
		p	***0.020**		***0.047**	***0.009**	0.087
Difference between correlations with PH-RSFC	Pearson r with decreased PH-PCC&RSC RSFC		-0.470	-0.491	-0.600	-0.396	**-0.734**
	Differce between PH RSFC-Ego Dissolution correlation and correlations with other VAS items	Z	-1.191	-1.111	-0.925	-1.809	
		p	0.117	0.133	0.178	***0.035**	

Table S7. Comparing correlations of imaging results with different ASC/VAS ratings: In the main text we describe the following significant correlations: V1 RSFC with complex imagery (ASC), V1 RSFC with elementary imagery (ASC), PH-RSC RSFC with altered meaning (ASC), increased CBF in visual areas with complex imagery (ASC), V1 RSFC with elementary hallucinations (VAS), and PH-RSC RSFC with ego-dissolution (VAS). In this table, these hypothesis-driven significant correlations are compared with correlations of the same results with different ASC or VAS scales (for which no-strong prior hypotheses were held). The term "selectivity" (used in the main article) is used to refer to a significant correlation (those displayed in Figs. 1-3 & S9) being greater in strength than a (spurious) non-hypothesised correlation. The z values represent the difference between correlations. The z values were calculated using a web-utility (1) that is based on the work of Steiger (1980) (2). Correlations related to the visual system and visual experiences are bordered in red and correlation related to the PH-RSC RSFC and ego-dissolution/altered meaning are bordered in blue. If these correlations are indeed "selective" we would expect them to differ significantly from those that fall outside of their borders and indeed this is largely the case. It can be seen from the table that the following correlations are highly selective: V1 RSFC with complex imagery (ASC), PH-RSC RSFC with altered meaning (ASC), increased CBF in visual areas with complex imagery (ASC), and V1 RSFC with elementary hallucinations (VAS). PH = parahippocampus; PCC = posterior cingulate cortex; RSC = retrosplenial cortex. * $p<0.05$, 1-tail.

		MNI_152 Coordinates		
	max (t)	*x*	*y*	*z*
Delta				
Temporoparietal Junction(L)	-4.43	-59	-65	18
Fusiform Gyrus (L)	-4.31	-35	-35	-29
Superior Temporal Gyrus (L)	-3.99	-65	-41	5
Theta				
Posterior Cingulate/RSC	-10.81	4	-40	13
Anterior Cingulate	-7.56	-1	28	26
Inferior Parietal(L)	-4.69	-37	-77	44
Angular Gyrus(L)	-4.42	-45	-73	28
Medial Frontal Gyrus(R)	-4.18	10	72	4
Precentral Gyrus (L)	-4.07	-29	-13	74
Middle Frontal Gyrus(L)	-3.8	-45	12	50
Superior Parietal Lobule(L)	-3.39	-37	69	52
Mid Frontal Orbital Gyrus(R)	-3.26	22	56	-13
Superior Frontal Gyrus(L)	-3.19	-27	42	19
Alpha				
Precuneus	-9.89	-3	-51	34
Anterior Cingulate	-6.11	-3	32	22
Precuneus	-4.26	-6	-35	56
Superior Occipital (L)	-4.08	-13	-99	32
Beta				
Middle Frontal Gyrus(L)	-9.31	-43	56	9
Posterior Cingulate	-8.54	0	-55	19
Superior Frontal Gyrus(R)	-7.29	12	64	11
Middle Temporal Gyrus(L)	-6.2	-66	-47	-7
Superior Temporal Gyrus(L)	-5.86	-63	-29	19
Superior Occipital Gyrus(R)	-5.31	10	-99	9
Mid Occipital Gyrus(L)	-5.3	-41	-77	36
Superior Occipital Gyrus(L)	-4.57	-5	-99	9
Superior Temporal Gyrus(L)	-4.5	-57	-55	19
Anterior Cingulate Gyrus	-4.41	-1	22	22

Table S8. Peak (MNI) coordinates from the MEG source localisation analysis (Figure 5). All between-condition differences are decreases in power, expressed as t-values.

Supplementary methods

Participants

All participants were recruited via word of mouth and provided written informed consent to participate after study briefing and screening for physical and mental health. The screening for physical health included electrocardiogram (ECG), routine blood tests, and urine test for recent drug use and pregnancy. A psychiatric interview was conducted and participants provided full disclosure of their drug use history. Key exclusion criteria included: < 21 years of age, personal history of diagnosed psychiatric illness, immediate family history of a psychotic disorder, an absence of previous experience with a classic psychedelic drug (e.g. LSD, mescaline, psilocybin/magic mushrooms or DMT/ayahuasca), any psychedelic drug use within 6 weeks of the first scanning day, pregnancy, problematic alcohol use (i.e. > 40 units consumed per week), or a medically significant condition rendering the volunteer unsuitable for the study.

Study setting and overview

Screening took place at Imperial's clinical research facility (ICRF) at the Hammersmith hospital campus. All study days were performed at Cardiff University Brain Research Imaging Centre (CUBRIC). Participants who were found eligible for the study attended two study days that were separated by at least 14 days. On one day, the participants received placebo, and on the other day they received LSD. The order of the conditions was balanced across participants, and participants were blind to this order but the researchers were not.

On scanning days, volunteers arrived at the study centre at 8:00am. They were briefed in detail about the study day schedule, gave a urine test for recent drug use and pregnancy, and carried out a breathalyser test for recent alcohol use. A cannula was inserted into a vein in the antecubital fossa by a medical doctor and secured. The participants were encouraged to close their eyes and relax in a reclined position when the drug was administered. All participants received 75 µg of LSD, administered intravenously via a 10ml solution infused over a two

minute period, followed by an infusion of saline. The administration was followed by an acclimatization period of approximately 60 minutes, in which (for at least some of the time) participants were encouraged to relax and lie with their eyes closed inside a mock MRI scanner. This functioned to psychologically prepare the participants for being in the subsequent (potentially anxiogenic) MRI scanning environment.

Participants reported noticing subjective drug effects between 5 to 15 minutes post-dosing, and these approached peak intensity between 60 to 90 minutes post-dosing. The duration of a subsequent plateau of drug effects varied among individuals but was generally maintained for approximately four hours post-dosing. MRI scanning started approximately 70 minutes post-dosing, and lasted for approximately 60 minutes. This included a structural scan, arterial spin labelling (ASL) fMRI, and BOLD fMRI. After the MRI scanning, there was a break of approximately 35 minutes, after which MEG scanning was performed. Once the subjective effects of LSD had sufficiently subsided, the study psychiatrist assessed the participant's suitability for discharge.

Scanning design and content

The ASL and BOLD scanning consisted of three eyes-closed resting state scans, each lasting seven minutes. After each seven minute scan, VAS ratings were performed in the scanner via a response-box. The first and third scans were eyes-closed rest but the second scan also incorporated listening to some music. This component of the study will be reported in detail in a separate publication. Prior to each scan, participants were instructed via onscreen instructions to close their eyes and relax. Participants also performed a retinotopic localisation paradigm at the end of the scanning session. This component of the study will be reported in more detail in a separate publication.

MEG scanning had a similar structure to the MRI, i.e. there were three eyes-closed resting-state scans with the second scan incorporating music listening, and there were three eyes-open resting-state scans, with the second incorporating the silent viewing of a movie. Again, the music, movie and eyes-open components of the study will be reported in detail in separate

publications. Finally, a mismatch negativity paradigm completed the protocol for the MEG scanning sessions, and this will be reported in another separate publication. In this paper, we report on the eyes-closed resting data which was collected with ASL, fMRI and MEG.

Subjective ratings

In scanner, VAS ratings were obtained after each scan. The scales included items for intensity, simple imagery, complex imagery, positive mood and ego dissolution and emotional arousal (Table S1). Specifically, they were phrased as follows: 1) "Please rate the intensity of the drug effects during the last scan", with a bottom anchor of "no effects", a mid-point anchor of "moderately intense effects" and a top anchor of "extremely intense effects"; 2) "With eyes closed, I saw patterns and colours", with a bottom anchor of "no more than usual" and a top anchor of "much more than usual"; 3) "With eyes closed, I saw complex visual imagery", with the same anchors as item 2; 4) "How positive was your mood for the last scan?", with the same anchors as item 2, plus a mid-point anchor of "somewhat more than usual"; 5) "I experienced a dissolving of my self or ego", with the same anchors as item 2; and 6) "Please rate your general level of emotional arousal for the last scan", with a bottom anchor of "not at all emotionally aroused", a mid-point anchor of "moderately emotionally aroused" and a top anchor of "extremely emotionally aroused". Since the ASC ratings referred to the peak drug effects and this coincided with the fMRI session (and not the MEG), ASC ratings were only included from the 15 participants who featured in the fMRI analyses (Fig. S1).

MRI

Anatomical Scans

Imaging was performed on a 3T GE HDx system. These were 3D fast spoiled gradient echo scans in an axial orientation, with field of view = 256 × 256 × 192 and matrix = 256 × 256 ×

192 to yield 1mm isotropic voxel resolution. TR/TE = 7.9/3.0ms; inversion time = 450ms; flip angle = 20°.

BOLD fMRI Data Acquisition

Two BOLD-weighted fMRI data were acquired using a gradient echo planer imaging sequence, TR/TE = 2000/35ms, field-of-view = 220mm, 64 × 64 acquisition matrix, parallel acceleration factor = 2, 90° flip angle. Thirty five oblique axial slices were acquired in an interleaved fashion, each 3.4mm thick with zero slice gap (3.4mm isotropic voxels). The precise length of each of the two BOLD scans was 7:20 minutes.

BOLD Pre-processing

Four different but complementary imaging software packages were used to analyse the fMRI data. Specifically, FMRIB Software Library (FSL) (3), AFNI (4), Freesurfer (5) and Advanced Normalization Tools (ANTS) (6) were used. One subject did not complete the BOLD scans due to anxiety and an expressed desire to exit the scanner and four others were discarded from the group analyses due to excessive head movement. Principally, motion was measured using frame-wise displacement (FD) (7). The criterion for exclusion was subjects with >15% scrubbed volumes when the scrubbing threshold is FD = 0.5. After discarding these subjects we reduced the threshold to FD = 0.4. The between-condition difference in mean FD for the 4 subjects that were discarded was 0.323±0.254 and for the 15 subjects that were used in the analysis the difference in mean FD was 0.046 ±0.032. The following pre-processing stages were performed: 1) removal of the first three volumes; 2) de-spiking (3dDespike, AFNI); 3) slice time correction (3dTshift, AFNI); 4) motion correction (3dvolreg, AFNI) by registering each volume to the volume most similar, in the least squares sense, to all others (in-house code); 5) brain extraction (BET, FSL); 6) rigid body registration to anatomical scans (twelve subjects with FSL's BBR, one subject with Freesurfer's bbregister and two subjects manually); 7) non-linear registration to 2mm MNI brain (Symmetric Normalization (SyN), ANTS); 8) scrubbing (8) - using an FD threshold of 0.4

(the mean percentage of volumes scrubbed for placebo and LSD was 0.4 ±0.8% and 1.7 ±2.3%, respectively). The maximum number of scrubbed volumes per scan was 7.1%) and scrubbed volumes were replaced with the mean of the surrounding volumes. Additional pre-processing steps included: 9) spatial smoothing (FWHM) of 6mm (3dBlurInMask, AFNI); 10) band-pass filtering between 0.01 to 0.08 Hz (3dFourier, AFNI); 11) linear and quadratic de-trending (3dDetrend, AFNI); 12) regressing out 9 nuisance regressors (all nuisance regressors were bandpassed filtered with the same filter as in step 10): out of these, 6 were motion-related (3 translations, 3 rotations) and 3 were anatomically-related (not smoothed). Specifically, the anatomical nuisance regressors were: 1) ventricles (Freesurfer, eroded in 2mm space), 2) draining veins (DV) (FSL's CSF minus Freesurfer's Ventricles, eroded in 1mm space) and 3) local white matter (WM) (FSL's WM minus Freesurfer's subcortical grey matter (GM) structures, eroded in 2mm space). Regarding local WM regression, AFNI's 3dLocalstat was used to calculate the mean local WM time-series for each voxel, using a 25mm radius sphere centred on each voxel (9).

fMRI motion correction

After discarding four subjects due to head motion, fifteen were left for the BOLD analysis. There was still a significant between-condition difference in motion for these subjects however (mean FD of placebo = 0.074 ±0.032, mean FD of LSD = 0.12 ±0.05, p = 0.0002). RSFC analysis is extremely sensitive to head motion (7) and therefore special consideration was given to the pre-processing pipeline to account for motion. This section goes into more detail about the pre-processing steps that were performed to reduce artefacts associated with motion as well as other non-neural sources of noise.

De-spiking has been shown to improve motion-correction and create more accurate FD values (10) and low-pass filtering at 0.08 Hz has been shown to perform well in removing high frequency motion (11). Six motion regressors were used as covariates in linear regression. It was decided that using more than six (e.g., "Friston 24-parameter motion regression" (12)) would be redundant and may impinge on neural signal (13) (especially

when other rigorous processes such as scrubbing (8) and local WM were applied (9)) . Using anatomical regressors is also a common step to clean noise and ventricles, DV and local WM were used in the pipeline employed in the present analyses. Local WM regression has been suggested to perform better than global WM regression (10).

It has previously been shown that head motion biases functional connectivity results in a distance-dependant manner (7). Therefore, as a quality control step, at the end of the pre-processing procedure, cloud plots were constructed to test for relationships between inter-node Euclidian distance and correlations between FD and RSFC across subjects. In cases in which motion is affecting the results, proximal nodes will have high FD-RSFC correlations and distal nodes will have low FD-RSFC correlations. This would result in a negative correlation between distance and FD-RSFC correlation. In the present dataset, the distance to FD-RSFC correlation was very close to zero for both the placebo and LSD conditions (Fig. S7), suggesting that the extensive pre-processing measures had successfully controlled for distance-related motion artefacts. The final quality control step was to correlate the results with mean FD across subjects (Table S6). Reassuringly, very few results correlated with mean motion (FD) and these were: vmPFC-PCC ($r = -0.48$, $p = 0.035$), V1-bilateral angular gyrus ($r = 0.56$, $p=0.015$). The significant correlation between changes in vmPFC-PCC RSFC and FD is also mentioned in (8) and (14); therefore, we decided not to elaborate on this result in the manuscript as it may have been an artifact of motion.

Seed-based RSFC

Based on prior hypotheses, 3 seeds were chosen for these analyses: 1) the bilateral parahippocampus (PH), vmPFC and V1. The PH seed was constructed by combining the anterior and posterior parahippocampal gyrus from the Harvard-Oxford probabilistic atlas and thresholded at 50%. The vmPFC seed was the same as one previously used by our team in analyses of psilocybin fMRI data (15) and MDMA fMRI data (16). The V1 seed was localized for each subject using a modified retinotopic scan. Specifically, subjects were presented with a 4:24 min video that alternated between vertical and horizontal polar angles (8 cycles, resolution=1400 x 1050, visual angle =23 x 23°, TR/TE=2000/25ms, 3mm

isotropic voxels). Fourier analysis with two distinct conditions was performed on the placebo data to identify activity corresponding to the vertical and horizontal polar angles (17). V1 was identified manually for each subject (using an in-house program). The vertical meridian served as the border between V1 and V2.

Mean time-series were derived for these seeds for each rest scan. The time series of V1 was derived from unsmoothed data because it was based on a functional localizer acquired in the subject's native space. RSFC analysis was performed using FSL's FEAT. Pre-whitening (FILM) was applied. A fixed-effects general linear modelling (GLM) was used to combine the results of both rest scans (2 x 7 mins) within a session. Subsequently, a higher level analysis was performed to compare placebo versus LSD conditions using a mixed-effects GLM (FLAME 1), cluster corrected ($z>2.3$, $p<0.05$). MRIcron was used to display the results.

Resting State Networks (RSN)

RSNs were derived using Independent Component Analysis (ICA) performed on data acquired separately as part of the Human Connectome Project (HCP) (18). All of the scans were pre-processed as part of the HCP (19). Two BOLD resting state scans (with opposite direction of phase encoding gradient) for 35 subjects were used in this analysis. Each scan was 14:33 minute long (TR/TE = 720/33.2ms, 2mm isotropic voxels). All scans were band-passed using the same filter as our BOLD scans (0.01 to 0.08 Hz). FSL's MELODIC was used to extract 20 ICA components. Out of these 20 ICA components, 12 were chosen as components of interest. These component were labelled: medial visual network (VisM), lateral visual network (VisL), occipital pole network (VisO), auditory network (AUD), sensorimotor network (SM), default-mode network (DMN), parietal cortex network (PAR), dorsal attention network (DAN), salience network (SAL), posterior opercular network (POP), left fronto-parietal network (lFP) and right fronto-parietal network (rFP).

Integrity (within-RSN RSFC)

Network integrity was calculated for each RSN for both placebo and LSD. All 20 HCP ICA spatial components were entered into FSL's dual regression analysis (20). The first step of the dual regression used the components as regressors applied to the 4D BOLD datasets for each subject, resulting in a matrix of time-series for each ICA. The second step involved regressing these time-series into the same 4D scan data to get a subject-specific set of spatial maps (parameter estimate (PE) images). For each subject, for each condition, and for each component, the PEs from the two rest scans in each run, were averaged. For each subject, for each condition, within each of the 12 RSNs of interest (threshold=3), the mean PE across voxels was calculated. This mean PE represents the integrity. Subsequently, paired t-tests were used to calculate the difference in integrity between conditions for each RSN (Bonferroni corrected for 12 RSNs).

Segregation (between-RSN RSFC)

Between-RSN RSFC was calculated in similar (although modified) manner to a previous analysis of ours involving psilocybin fMRI data (21). Specifically, a 12x12 matrix was constructed that represents RSFC between different RSN pairs. For each subject, for each condition, the time-series (from the first step of the dual regression, detailed above) for each pair of RSNs, were entered into a GLM, resulting in a PE value representing the strength of functional connectivity between each pair of RSNs. GLM was used rather than correlation coefficients because differences between Pearson's correlations could be a result of either signal or noise differences; therefore, it is preferable to perform regression and look for drug-placebo differences on the PE (22). The GLM was estimated twice: 1) each RSN as a dependant variable in one model, and 2) each RSN as an independent variable in the second model. These two PE values were then averaged together, to generate a symmetric 12 x12 matrix (Fig. 4b). Three 12 x 12 matrices were created as follows: 1) the group mean PE values for placebo, 2) the group mean PE values for LSD, and 3) paired t-test to compare the PE values for the two conditions, LSD and placebo (two-tailed, 5000 permutations).

Variance

It has been recently proposed that moment-to-moment brain signal variability contains important information about neurophysiological processes that may be more informative than other traditional metrics such as mean signal values (23, 24). Furthermore, the association of high temporal variability with regions of high metabolism in cortical grey matter (25) and its parametric modification by task difficulty (26) suggest a direct relationship with ongoing neural processing. Here, the effects of LSD on the temporal variability of the average BOLD signal from each RSN were investigated using the standard definition of variance of a time series series $\mathrm{Var}(\mathrm{X}) = < (\mathrm{X} - < \mathrm{X} >)^2 >$ (where <,> denotes the temporal average). According to this definition, $\mathrm{Var}(\mathrm{X}) = 0$ only for a constant time series and larger fluctuations around the mean imply larger values of the variance.

Cerebral blood flow

The ASL time series were motion corrected using *3dvolreg* within AFNI. Brain extraction was performed after correcting for coil sensitivity profiles by spatially regressing the 3rd-order polynomial fit of the minimal contrast data from the ASL time series data. Masks of the lateral ventricles were determined from the structural scan and the average value of the calibration scan within these masks was defined as $M_{0,CSF}$. The equilibrium magnetisation for arterial blood ($M_{0,blood}$) was then calculated according to methods previously described (27). For each TI, tag and control time series were separately interpolated to the TR, subtracted and averaged. CBF and arterial arrival times were quantified by fitting a general kinetic model (28) to the resulting multi-TI data using a non-linear fitting routine and the calculated $M_{0,blood}$. The CBF maps were registered to the BOLD data and transformed to standard space using the same ANTS transformations as described above.

Bonferroni correction for correlations

For correlations between imaging outcomes and subjective ratings related to visual hallucinations, Bonferonni correction by a factor of 4 was applied (there were 4 items related to visual hallucinations - two from ASC and two from VAS). For imaging outcomes correlated with the VAS measure of ego-dissolution, no correction was applied, as no other VAS items were used in exploratory correlational analyses. For correlations between imaging outcomes and the different dimensions of the ASC, correction by a factor of 11 was applied, as these analyses were exploratory and there are 11 dimensions to the ASC.

MEG

MEG recordings

For the MEG recordings, participants lay in supine position. Participants' pulse rate and blood oxygenation level were continually monitored throughout the experiment via a probe over their left hand index finger. Whole-head MEG recordings were made using a CTF 275-channel radial gradiometer system sampled at 1200 Hz (0–300 Hz band-pass). An additional 29 reference channels were recorded for noise cancellation purposes and the primary sensors were analysed as synthetic third-order gradiometers. Four of the 275 channels were turned off due to excessive sensor noise. In addition to the MEG channels, we recorded participants' ECG: horizontal and vertical electro-oculograms as well as electromyograms from bilateral frontalis and temporalis muscles. Participant compliance was also monitored via an eye-tracking camera. Seven minutes of resting-state data were recorded in each block after which the VAS scales were completed. Continuous monitoring of participant head position was employed using three fiducial coils (nasion and pre-auricular points).

Data Preprocessing

All MEG recordings were initially high-pass filtered at 1 Hz, and segmented into epochs of 2 s in length (210 epochs). Each epoch was then visually inspected, and those with gross

artifacts (e.g., head movements, jaw clenches) were removed from the analysis. An automated algorithm was used to remove further epochs contaminated with muscle artefacts. In this algorithm, a set of 30 gradiometer sensors were predefined at the edge of the MEG dewar, as these are most likely to be contaminated by muscle artefacts (29). Using Hanning-windowed fourier transformations, we calculated the mean spectral power for these sensors in the 105-145Hz frequency band for each epoch. If the resulting power averaged across these sensors exceeded 10 fT (29) then that epoch was eliminated from subsequent analysis. On the remaining epochs we then performed independent component analysis (ICA) as implemented in Fieldtrip/EEGLAB (30, 31) to identify and remove ocular, muscle and cardiac artifacts from the data. Any components that showed a correlation ($r > .10$) in the time domain with the EOG/EMG electrodes were automatically removed. Likewise, any components that showed correlations ($r > .10$) with similarly filtered EOG/EMG channels after being bandpass filtered in the range 105-145 Hz were removed. Visual inspection was also used to remove artifact components. All subsequent sensor space analysis was performed on the ICA cleaned datasets. Of the twenty participants, one was unable to complete both sessions and a further five were discarded due to the presence of excessive muscle artefacts that could not be satisfactorily removed by ICA, or due to excessive head motion.

Frequency analysis – sensor space

Using the FieldTrip toolbox (31) we converted our MEG data to planar gradient configuration and then conducted a frequency analysis of the individual vector directions. Frequency analysis was conducted using Hanning windowed fast Fourier transforms between 1 and 30 Hz at 0.5 Hz frequency intervals and then the planar directions combined to give local maxima under the sensors. Analysis of sensor-level MEG data in a planar gradient (spatial-derivative) configuration has the advantage of easy interpretability, because field maps can be interpreted as having a source directly underneath field maxima (32). For the higher frequency bands (30-100 Hz) we employed frequency analysis using slepian multitapers with spectral smoothing +/- 3 Hz (33). For statistical analysis, we divided individual spectra into the following frequency bands: delta (1 - 4 Hz), theta (4- 8 Hz), alpha

(8 - 15 Hz), beta (15 - 30 Hz), low gamma (30 - 49 Hz), and high gamma (51 - 99 Hz) (29). A relatively high upper alpha frequency cut-off (15 Hz) was used as preliminary analyses revealed a striking peak shift in the alpha-band frequency (Fig. 5c). The differences between LSD and placebo were tested using permutation testing of t statistics (34, 35). The Type 1 error rate was controlled using cluster randomization analysis with an initial cluster-forming threshold of $p = 0.05$ repeated over 5000 permutations.

MEG Source Localization

Automated segmentation and labeling was performed for each individual MRI using the Freesurfer software package (36). Leadfield matrices were then computed on the resultant meshes for each subject using the overlapping spheres method (37). This method models cortical spheres beneath each sensor with elementary current dipoles estimated on a grid perpendicular to the cortical surface. Each individual forward model comprised 10,000 vertices. Noise covariance matrices were computed from empty room recordings. Before calculating the source kernel an additional head-cleaning procedure was performed. Transient head movements greater than 5mm were discarded, while significant repositioning of the head during the scan was dealt with by slicing the recording into discreet units, computing the forward solution for each, and concatenating the resultant sources. Source time-series were obtained by calculating an unconstrained kernel using the dynamical statistical parametric mapping (dSPM) method implemented in the open-source software Brainstorm (38). dSPM is a normalized implementation of the generalized minimum-norm solution (MNE) (39), which has been optimized to resolve the MNE inverse solution's characteristic bias toward the sensors. dSPM and other normalized minimum norm solutions have shown to be less susceptible to dipole localization error than standard or weighted MNE, and yield more accurate estimates of deep lateral and midline sources of interest such as insular, fusiform, cingulate, and parahippocampal gyri (40). Dipoles were assumed not to have fixed orientation, eliminating the necessity of artificial post-hoc smoothing. Following source computation, data were band-pass filtered into frequencies of interest and projected into standard MNI space. Time- course normalization was conducted for each subject by

subtracting the voxel mean from each voxel time-point and dividing by the standard deviation. Data were then exported to SPM for statistical comparison. A paired t-test was run for all frequency conditions, comparing the LSD vs placebo time-courses. Error corrections were performed using False discovery rate (FDR) procedure, thresholded at $p = 0.05$.

Author contributions

R.C-H designed and led the study, oversaw recruitment, performed the research and wrote the paper. D.J.N. advised on the study's design and implementation and edited the paper. A.F. was instrumental in initiating the research and edited the paper. M.K. helped design the study, recruit volunteers, analyse the MEG data and perform and coordinate the research. S.D.M. helped design the study, performed the MEG analyses and the research itself and wrote sections of the paper, including that on MEG. L.R., E.T. and K.M. performed the fMRI analyses and wrote sections of the paper. L.R., R.L, C.O., J.M. and E.T. oversaw the BOLD analyses. L.R., R.C-H and E.T. were instrumental in producing and arranging the fMRI figures. P.He. helped with the fMRI analyses. K.M oversaw the CBF analysis and L.R. helped with performing this analysis. S.D.M., T.C.N., E.E.S. and M.K. all contributed to the MEG analyses with S.D.M. overseeing its implementation. T.C.N. performed the source-localisation analyses and oversaw this aspect of the MEG analyses. L.T.J.W., T.M.W., M.B., B.S. helped perform the research and care for the participants. T.M.W., M.B., B.S. administered the LSD and served as medical/psychiatric cover for the study. H.V.C. oversaw the storage of the LSD. D.E.N. advised on the stability of and storage conditions for the LSD. R.W., K.S. and J.E. advised on the MRI and MEG scanning design and oversaw CUBRIC's hosting of the study. P.Ho. was the principal radiographer for the MRI and W.D. ran most of the MEG sessions. M.I.S. oversaw the retinotopic localisation and L.R. implemented this and performed the relevant analyses.

References

1. Lee IA & Preacher KJ (2013) Calculation for the test of the difference between two dependent correlations with one variable in common *[Computer software]*.
2. Steiger JH (1980) Tests for comparing elements of a correlation matrix. *Psychological Bulletin* 87:245-251.
3. Smith SM*, et al.* (2004) Advances in functional and structural MR image analysis and implementation as FSL. *Neuroimage* 23:S208-S219.
4. Cox RW (1996) AFNI: software for analysis and visualization of functional magnetic resonance neuroimages. *Computers and Biomedical research* 29(3):162-173.
5. Dale AM, Fischl B, & Sereno MI (1999) Cortical surface-based analysis: I. Segmentation and surface reconstruction. *Neuroimage* 9(2):179-194.
6. Avants BB, Tustison N, & Song G (2009) Advanced normalization tools (ANTS). *Insight J* 2:1-35.
7. Power JD*, et al.* (2014) Methods to detect, characterize, and remove motion artifact in resting state fMRI. *Neuroimage* 84:320-341.
8. Power JD, Barnes KA, Snyder AZ, Schlaggar BL, & Petersen SE (2012) Spurious but systematic correlations in functional connectivity MRI networks arise from subject motion. *Neuroimage* 59(3):2142-2154.
9. Jo HJ, Saad ZS, Simmons WK, Milbury LA, & Cox RW (2010) Mapping sources of correlation in resting state FMRI, with artifact detection and removal. *Neuroimage* 52(2):571-582.
10. Jo HJ*, et al.* (2013) Effective preprocessing procedures virtually eliminate distance-dependent motion artifacts in resting state FMRI. *Journal of applied mathematics* 2013.
11. Satterthwaite TD*, et al.* (2013) An improved framework for confound regression and filtering for control of motion artifact in the preprocessing of resting-state functional connectivity data. *Neuroimage* 64:240-256.
12. Friston KJ, Williams S, Howard R, Frackowiak RS, & Turner R (1996) Movement-related effects in fMRI time-series. *Magnetic resonance in medicine* 35(3):346-355.
13. Bright MG & Murphy K (2015) is fMRI "noise" really noise? Resting state nuisance regressors remove variance with network structureI. *NeuroImage* 114:158-169.
14. Van Dijk KR, Sabuncu MR, & Buckner RL. (2012) The influence of head motion on intrinsic functional connectivity MRI. *Neuroimage* 59(1):431-438.
15. Carhart-Harris RL*, et al.* (2012) Functional Connectivity Measures After Psilocybin Inform a Novel Hypothesis of Early Psychosis. *Schizophrenia bulletin*.
16. Carhart-Harris RL*, et al.* (2014) The effects of acutely administered MDMA on spontaneous brain function in healthy volunteers measured with arterial spin labelling and BOLD resting-state functional connectivity *Biological Psychiatry*.
17. Sereno MI*, et al.* (1995) Borders of multiple visual areas in humans revealed by functional magnetic resonance imaging. *Science* 268(5212):889-893.
18. Van Essen DC*, et al.* (2013) The WU-Minn human connectome project: an overview. *Neuroimage* 80:62-79.
19. Glasser MF*, et al.* (2013) The minimal preprocessing pipelines for the Human Connectome Project. *Neuroimage* 80:105-124.
20. Beckmann CF, Mackay CE, Filippini N, & Smith SM (2009) Group comparison of resting-state FMRI data using multi-subject ICA and dual regression. *Neuroimage* 47(Suppl 1):S148.

21. Roseman L, Leech R, Nutt DJ, Feilding A, & Carhart-Harris RL (2014) The effects of psilocybin and MDMA on between-network resting state functional connectivity in healthy volunteers. *Frontiers in human neuroscience* 8.
22. Friston KJ (2011) Functional and effective connectivity: a review. *Brain connectivity* 1(1):13-36.
23. Garrett DD*, et al.* (2013) Moment-to-moment brain signal variability: a next frontier in human brain mapping? *Neuroscience & Biobehavioral Reviews* 37(4):610-624.
24. Garrett DD, Kovacevic N, McIntosh AR, & Grady CL (2010) Blood oxygen level-dependent signal variability is more than just noise. *The Journal of Neuroscience* 30(14):4914-4921.
25. Tagliazucchi E*, et al.* (2013) Breakdown of long-range temporal dependence in default mode and attention networks during deep sleep. *Proceedings of the National Academy of Sciences* 110(38):15419-15424.
26. Garrett DD, McIntosh AR, & Grady CL (2014) Brain signal variability is parametrically modifiable. *Cerebral Cortex* 24(11):2931-2940.
27. Wong EC, Buxton RB, & Frank LR (1998) Quantitative imaging of perfusion using a single subtraction (QUIPSS and QUIPSS II). *Magnetic resonance in medicine : official journal of the Society of Magnetic Resonance in Medicine / Society of Magnetic Resonance in Medicine* 39(5):702-708.
28. Buxton RB*, et al.* (1998) A general kinetic model for quantitative perfusion imaging with arterial spin labeling. *Magnetic resonance in medicine : official journal of the Society of Magnetic Resonance in Medicine / Society of Magnetic Resonance in Medicine* 40(3):383-396.
29. Muthukumaraswamy SD, Shaw AD, Jackson, LE, Hall J, Moran R, & Saxena N (2015). Evidence that subanesthetic doses of ketamine cause sustained disruptions of NMDA and AMPA-mediated frontoparietal connectivity in humans. *The Journal of Neuroscience* 35(33):11694-11706.
30. Delorme A & Makeig S (2004) EEGLAB: an open source toolbox for analysis of single-trial EEG dynamics including independent component analysis. *Journal of neuroscience methods* 134(1):9-21.
31. Oostenveld R, Fries P, Maris E, & Schoffelen JM (2011) FieldTrip: Open source software for advanced analysis of MEG, EEG, and invasive electrophysiological data. *Computational intelligence and neuroscience* 2011:156869.
32. Bastiaansen MC & Knosche TR (2000) Tangential derivative mapping of axial MEG applied to event-related desynchronization research. *Clinical neurophysiology : official journal of the International Federation of Clinical Neurophysiology* 111(7):1300-1305.
33. Mitra PP & Pesaran B (1999) Analysis of dynamic brain imaging data. *Biophysical journal* 76(2):691-708.
34. Nichols TE & Holmes AP (2002) Nonparametric permutation tests for functional neuroimaging: a primer with examples. *Human brain mapping* 15(1):1-25.
35. Maris E & Oostenveld R (2007) Nonparametric statistical testing of EEG- and MEG-data. *Journal of neuroscience methods* 164(1):177-190.
36. Fischl B (2012) FreeSurfer. *NeuroImage* 62(2):774-781.
37. Huang MX, Mosher JC, & Leahy RM (1999) A sensor-weighted overlapping-sphere head model and exhaustive head model comparison for MEG. *Physics in medicine and biology* 44(2):423-440.

38. Tadel F, Baillet S, Mosher JC, Pantazis D, & Leahy RM (2011) Brainstorm: a user-friendly application for MEG/EEG analysis. *Computational intelligence and neuroscience* 2011:879716.
39. Dale AM*, et al.* (2000) Dynamic statistical parametric mapping: combining fMRI and MEG for high-resolution imaging of cortical activity. *Neuron* 26(1):55-67.
40. Hauk O, Wakeman DG, & Henson R (2011) Comparison of noise-normalized minimum norm estimates for MEG analysis using multiple resolution metrics. *NeuroImage* 54(3):1966-1974.